SMAR 2017 – Fourth Conference on Smart Monitoring,
Assessment and Rehabilitation of Civil Structures

SMAR 2017

Interfacial cohesive material law for SRP strips bonded to concrete

Christian Carloni[1], Mattia Santandrea[1], and Imohamed Ali Omar Imohamed[1]

[1] Department of Civil, Chemical, Environmental, and Materials Engineering, University of Bologna, Viale Risorgimento 2, 40126, Bologna, Italy

ABSTRACT: Steel reinforced polymer (SRP) composites is a new system in the toolbox of strengthening and rehabilitation techniques for existing buildings. SRP systems consist of ultra-high-strength steel cords embedded in a thermosetting epoxy resin. This new tool combines the convenience of low cost steel cords with the advantage of high strength fibers that allow it to be a successful alternative with respect to other fiber-reinforced polymer (FRP) composite systems. In this work, the stress transfer mechanism between SRP and concrete substrate is studied. SRP composite strips are bonded to concrete prisms and tested using a single-lap shear test setup. Load responses are presented and failure modes are discussed. The influence of different densities of steel cords on the load response and failure modes is examined. Digital image correlation (DIC) is used to compute the strain field on the surface of the composite strip, which allows to determine directly the interfacial cohesive material law.

1 INTRODUCTION

The use of new strengthening systems to repair and rehabilitate existing concrete buildings has experienced a significant increase in the last decades, inducing researchers to explore the effectiveness of these emerging techniques. Concrete structures usually suffer damages or reductions in the member load capacities due to ageing of the materials or natural hazards, such as earthquakes. In an attempt to preserve the existing building heritage, fiber reinforced polymer (FRP) composites became popular at the end of the twentieth century, for strengthening and rehabilitation applications of existing reinforced concrete buildings. FRP composites offer several advantages with respect to traditional strengthening systems, such as ease of installation, high strength-to-weight ratio, high corrosion resistance, and minimal change in dimension of the strengthened member. The interfacial debonding mechanism between FRP composites and a concrete substrate is the most common failure mode observed for this type of strengthening systems and has been widely investigated by several research groups, such as Chajes et al. (1996), Taljsten (1997), Bizindavyi et al. (1999), Nakaba et al. (2001), Savoia et al. (2003), and Dai et al. (2003). Recently, newly-developed composites, known as steel-FRPs or steel reinforced polymer (SRP) composites, have been introduced as an appealing alternative to traditional FRPs (Casadei et al. 2005, Huang et al. 2005, Matana et al. 2005). The low cost of the steel fibers compared with carbon or aramid fibers makes SRP a competitive composite material. SRP composites consist of ultra-high strength steel fibers embedded in an organic matrix. The available literature highlights the potentials of SRPs to improve the structural performances of concrete structures (Wobbe et al. 2004, Barton et al. 2005, Huang et al. 2005, Pecce et al. 2006, Prota et al. 2006, Lopez et al. 2007, Saber et al. 2008, Mitolidis et al. 2012, Balsamo et al. 2013, Bencardino et al. 2014, De Santis et al. 2016).

In this work, the stress transfer mechanism between SRP and concrete substrate is studied. SRP composite strips are bonded to concrete prisms and tested using a single-lap shear test setup. Digital image correlation (DIC) is used to qualitatively and quantitatively study the strain field on the surface of the composite strip in order to obtain the interfacial cohesive material law.

2 EXPERIMENTAL PROGRAM

2.1 Materials

One single batch of concrete was employed to cast the concrete prisms used for direct shear tests as well as the other specimens to determine the mechanical properties of the material. The maximum aggregate size was equal to 15 mm. Compressive and tensile strengths of concrete was measured at 21 (only cubes were tested), 28, 42, 56, 84, 112, 168, 224, and 420 days after casting using 150 mm side cubes (compression) and 150 mm × 300 mm cylinders (splitting) tested according to EN 12390-3 and EN12390-6, respectively. In addition, 150 mm × 300 mm concrete cylinders were tested in compression at 84, 112, 168, 224, and 420 days after casting according to EN 12390-3. The average values of 3 tests for each day are plotted in Figure 1.

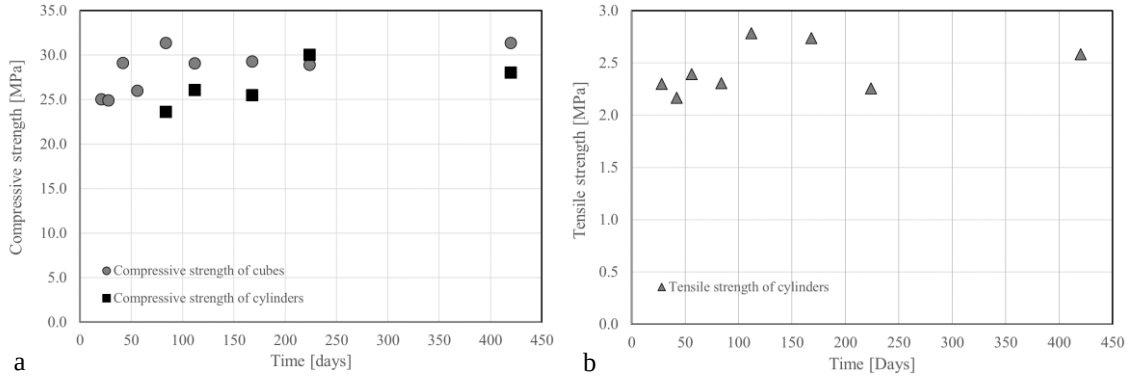

Figure 1. Concrete strength gain: a) compressive strength, b) tensile strength.

Three notched concrete prisms 600 mm length × 150 mm width × 150 mm depth and three notched concrete prisms 300 mm length × 75 mm width × 75 mm depth were tested at approximately 300 days using a three point bending set-up to evaluate the fracture energy of concrete. The fracture mechanics set-up and details about fracture tests are reported in Santandrea et al. (2017). The fracture energy was found equal to 0.104 N/mm (CoV 0.05) and 0.109 N/mm (CoV 0.12) for 600 mm × 150 mm × 150 mm prisms and 300 mm × 75 mm × 75 mm prisms, respectively. The value of G_F obtained from experimental tests can be compared with the value obtained from the formula proposed by Taerwe et al. (2013) that resulted equal to 0.132 N/mm. Experimental results seemed in good agreement with the predictive formula.

The composite material consisted of steel fibers strip embedded in a polymeric matrix. Steel fibers were in the form of a unidirectional sheet made of ultra-high strength galvanized steel micro-cords (Kerakoll 2017). The cross-sectional area of the cord A_{cord} is 0.538 mm^2. Two different fiber densities were investigated, i.e. high density (HD) and ultra-high density (UHD) steel fibers. The numbers of cords per mm is equal to 0.472 and 0.709 for HD and UHD steel sheets, respectively. The epoxy matrix is a two-component epoxy thixotropic gel system. The mechanical properties of fibers and matrix are provided in Table 1 and Table 2, respectively.

Table 1. Properties of steel fibers provided by manufacturer (Kerakoll 2017).

Steel fibers	Number of cords/mm	Tensile strength [MPa]	Elastic Modulus [GPa]	Break Deformation [%]	Equivalent thickness [mm]
High density (HD)	0.472	> 3000	> 190	> 2	≈ 0.254
Ultra-high density (UHD)	0.709	> 3000	> 190	> 2	≈ 0.381

Table 2. Mechanical properties of epoxy provided by manufacturer (Kerakoll 2017).

Matrix	Tensile strength	Flexural elastic modulus	Elastic modulus under compression
Epoxy	> 14 MPa	> 2.50 GPa	> 5.30 GPa

2.2 Methods

Ten SRP-concrete joints were tested using the single-lap shear test set-up in order to investigate the debonding mechanism between the composite strips and the concrete surface and determine the interfacial cohesive material law (CML), which represent the relationship between the shear stress transferred at the interface and the slip between two points of the interface on the opposite surface of the crack. All concrete prisms were sandblasted with silica sand prior to applying the SRP strips. A wet layup process was used to apply the SRP strip to the concrete surface. Specimens were left to cure in the laboratory for seven days after casting. SRP strips were externally bonded to one face of the concrete prisms. The classical push-pull configuration was adopted where composite was pulled while the concrete prism was restrained. The dimensions of all concrete blocks were 150 mm with × 150 mm depth × 600 mm length. The epoxy resin was used to impregnate the fiber along the entire SRP strip, i.e. also outside the bonded area. The thickness of each layer of matrix was 2 mm, thus, the total thickness of the composite was equal to 4 mm. The bonded area started 70 mm from the top edge (loaded end of the strip) of the concrete prism to obtain an initial interfacial notch. The FRP strips were directly gripped by the machine head. Direct shear tests were conducted under displacement control using a close-loop servo-hydraulic universal testing machine (Figure 2).

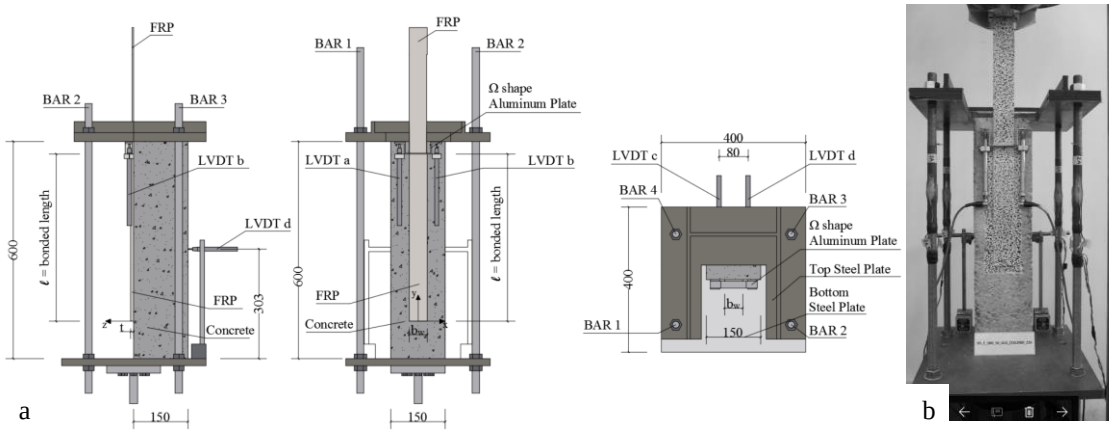

Figure 2. Test set-up: a) Sketch, b) Photo.

Two linear variable differential transducers (LVDT) were mounted on the concrete surface close to the top edge of the bonded region. The LVDTs (named LVDT a and b) reacted off of a thin aluminum Ω-shaped bent plate that was attached to the epoxy surface adjacent to the beginning of the bonded area. The average of LVDT a and b is defined as global slip *g* in this paper. *g* was increased at a constant rate equal to 0.00084 mm/s. Two additional LVDTs (named LVDT c and d) were used to monitor the horizontal displacement of the concrete prism in the direction perpendicular to the face of the composite strip. Additional information on the test setup can be found elsewhere (Santandrea et al. 2016). Three-dimensional (3D) digital image correlation (DIC) was used for all specimens to obtain the displacement field and consequently derive the strain field on the SRP strip surface (Carloni et al. 2010). Single-lap shear tests were conducted varying the density of steel fibers. Bonded width and bonded length were kept constant and equal to 50 mm and 300 mm, respectively. For each concrete prism, all three longitudinal formed faces were used to apply the SRP strip. The face opposite to the casting one was named bottom (B) face, the ones adjacent to the casting one were termed side (S) faces. Specimens were named following the notation DS-X-Y-A-B-Z, where X = bonded length (ℓ) in mm, Y = bonded width (b_f) in mm, A represents the steel fiber density (HD = high density, UHD = ultra-high density), B denotes the face of the block to which the SRP strip was applied (B = bottom, S = side), and Z = specimen number. Specimen are listed in Table 3.

3 TEST RESULTS

The direct shear test load responses of representative specimens, characterized by different densities and different face of application of the SRP strips, are plotted in Figure 3a. The shape of all load responses is similar. The initial linear response is followed by a non-linear branch until a peak is reached. A sudden drop in the load after the peak marks the onset of the interfacial crack propagation. As the crack propagates, the load remains nominally constant. The global slip range (g_1,g_2) in which the load attains a constant value, varies slightly for each test and is determined on the basis of the strain analysis results (presented in the next session). The failure mode of all SRP concrete joints was the debonding of the composite strip from the concrete substrate. A thin layer of concrete remained attached to the epoxy matrix for the entire length of the SRP strip. At the free end (i.e., the end of the strip opposite to the end where the load was applied), a bulb of concrete remained attached to the composite strip at the free end due to the presence of fracture mechanics Mode-I loading condition. The detachment of the concrete bulb from the substrate determines an increase in the amount of energy needed to fully detach the strip, which causes an ascending branch in the last portion of almost all the load responses. Figure 3b and 3c show the failure mode for specimen DS_300_50_HD_B_1.

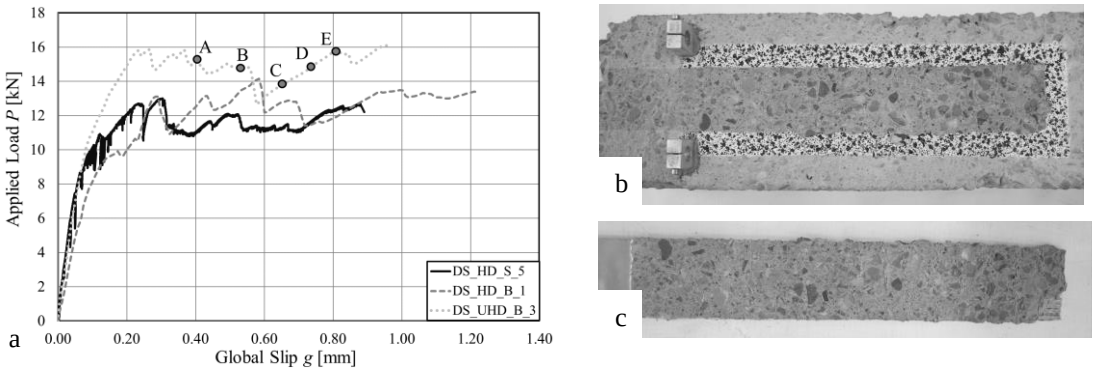

Figure 3. a) Load responses of representative specimens, b) and c) Failure mode of specimen DS_300_50_HD_B_1.

4 DISCUSSION OF RESULTS

4.1 Strain analysis in direct-shear tests

In this study, DIC was used to obtain the strain profile on the surface of the SRP strip in the direction of the fibers. Displacements field was obtained for different square areas (subsets) for a 5 pixel step size, which provided points spaced at approximately 1.67 mm. Different subsets of 21, 31, and 41 pixels were used to study the influence of subset dimension on the displacement field. Results determined using different subsets are similar, therefore a subset size of 21 pixels (approximately 7 mm) edge was employed to carry out the analysis presented in this section. The strain analysis reported in this section refers to the Cartesian system shown in Fig. 2a. The values of the longitudinal strain ε_{yy} were determined along the center line of the SRP strip by averaging the strain across a 15mm-wide strip for each value of *y*. Averaging the strain across a 15 mm width allow for taking into account the variation of the strain due to the presence of a non-homogeneous substrate and local material variations in the SRP strip. A 15-mm strip was chosen based on the aggregate size. The experimental nonlinear strain distribution along the bonded length was approximated using the equation proposed by Dai et al. (2005):

$$\varepsilon_{yy}(y) = \frac{R\exp\left(P\left(Ry+T\right)\right)}{\exp\left(P\left(Ry+T\right)\right)+1} \tag{1}$$

Where R, P, and T are parameters evaluated through a non-linear regression analysis of the strains obtained from DIC. The strain distribution during the debonding process can be divided into three main regions: (a) the stress-free zone (SFZ); (b) the stress-transfer zone (STZ); and (c) the fully-debonded zone (FDZ). The stress transfer occurs in the STZ, usually characterized by an S-shaped strain profile. In the FDZ the composite strip is completely debonded from the concrete substrate, i.e. no shear transfer is transferred and the strains are essentially constant. The SFZ is localized in the portion of the SRP strip near the free end and represents the part of the composite strip not yet affected by the shear transfer. While the global slip increases during the debonding mechanism, the S-shaped strain profile shifts gradually from the loaded end to the free end of the composite strip, and the FDZ advances as well while the strain in the FDZ remains constant (ε_{max}). For each test, the global slip range (g_1,g_2) was defined as the range where the S-shaped profile was fully established. Figure 4a represents the strain profiles of specimen DS_300_50_UHD_B_3 obtained at 5 different values of the global slip (showed in Figure 3a), fitting the experimental values with Eq. (1). The 5 points identified in Figure 3a correspond to 5 different images analyzed with DIC. It can be observed that a simple translation of the STZ along the length of the SRP strip occurred as the global slip increased while its shape remained constant.

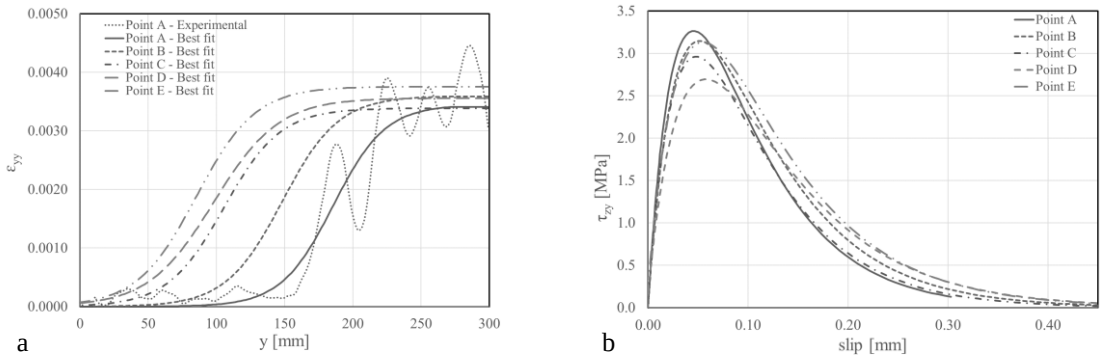

Figure 4. a) Strain profiles and b) cohesive material laws of specimen DS-300_50_UHD_B_3.

4.2 Interfacial cohesive material law

The value of the shear stress at any location of the composite strip can be defined from the analytical equations representing the strain profile, using the following relationship:

$$\tau_{zy}(y) = E_f t_f \frac{d\varepsilon_{yy}}{dy} \tag{2}$$

where E_f and t_f are respectively the elastic modulus and the thickness of the fibers. The slip between the SRP strip and the concrete substrate at any location of the composite strip can be evaluated from the strain profile:

$$s(y) = \int_0^y \varepsilon_{yy} dy \tag{3}$$

Dai et al. (2005) proposed an analytical formula to relate the shear stresses and the corresponding slip for a composite strip bonded to a concrete surface, termed cohesive material law (CML) and associated to the strain profile provided in Equation (1):

$$\tau_{zy} = R^2 P E_f t_f \exp(-Ps)(1-\exp(-Ps)) \tag{4}$$

where R and P are the parameters obtained from the non-linear regression of the strain profile, as defined above. Figure 4b represents the CMLs for specimen DS_300_50_UHD_B_3 obtained from the fitted strain profiles showed in Figure 4a. The fracture energy, G_F, i.e. the energy required to fully break the elementary unit area of the cohesive crack, corresponds to the area under the entire τ_{zy}(s) curve:

$$G_F = \int \tau_{zy}(s) ds \tag{5}$$

Table 3 summarizes, for each specimen, the value of the maximum strain along the SRP strip in the FDZ, ε_{max}, the maximum shear stress, τ_{max}, the slip corresponding to the maximum shear stress, s_m, and the fracture energy G_F.

Table 3. Cohesive material law parameters obtained from DIC analysis (Cov is reported within parenthesis).

Specimen name	ε_{max}	τ_{max} [MPa]	s_m [mm]	G_F [N/mm]	Number of cords
DS_300_50_HD_S_1	0.0044 (0.06)	2.9 (0.17)	0.06 (0.19)	0.47 (0.11)	24
DS_300_50_HD_S_2	0.0042 (0.06)	3.2 (0.13)	0.05 (0.17)	0.42 (0.11)	24
DS_300_50_HD_S_3	0.0042 (0.06)	2.4 (0.19)	0.06 (0.07)	0.43 (0.17)	24
DS_300_50_HD_S_4	0.0035 (0.07)	2.3 (0.11)	0.05 (0.12)	0.30 (0.14)	24
DS_300_50_HD_S_5	0.0038 (0.06)	3.3 (0.10)	0.04 (0.12)	0.36 (0.12)	24
DS_300_50_HD_B_1	0.0041 (0.06)	3.4 (0.22)	0.04 (0.16)	0.42 (0.11)	24
DS_300_50_HD_B_2	0.0042 (0.06)	2.9 (0.16)	0.05 (0.19)	0.42 (0.12)	24
DS_300_50_UHD_B_1	0.0036 (0.05)	5.3 (0.29)	0.04 (0.35)	0.48 (0.10)	35
DS_300_50_UHD_B_2	0.0041 (0.06)	3.5 (0.30)	0.07 (0.29)	0.62 (0.13)	35
DS_300_50_UHD_B_3	0.0035 (0.06)	3.3 (0.20)	0.05 (0.25)	0.43 (0.12)	35

The value of each parameter, for each test, is obtained as the mean value calculated from a minimum of ten points of the load response within (g_1,g_2), which correspond to ten images of DIC. Comparing specimens with HD steel fibers applied to two different faces (S or B), the fracture energy, G_F, seems to vary. The average value of G_F, for S-face HD specimens is equal to 0.39 N/mm and it is lower than the average value obtained for B-face HD specimens, which is equal to 0.42 N/mm. Two UHD specimens out of three, tested on B-face, showed similar values of the fracture energy, G_F, (0.48 N/mm and 0.43 N/mm) with respect to HD specimens tested on B-face (0.42 N/mm for both specimens).

5 CONCLUSIONS

This paper presents the results of an experimental study carried out to investigate the CML of SRP composite strips applied to a concrete prism. Direct shear tests were conducted on specimens, varying the face of application of the composite strip and the density of steel fibers. The following conclusions can be drawn from the results:

1) The strain profile of SRP composite strips bonded to a concrete substrate is S-shaped as it is typically observed for FRP composites applied to quasi-brittle substrates. During the debonding process, the strain profile shifts in a self-similar manner to the free end of the SRP strip, without changing its shape.
2) High density SRP strips bonded to the bottom face of the concrete prism show an increase of the interfacial fracture energy with respect to S-face HD specimens. Similar values of the fracture energy are observed comparing B-face UHD specimens with B-face HD specimens.

6 AKNOLEDGEMENTS

The experimental work presented in this paper was conducted in the laboratory of structural and geotechnical engineering (LISG) at the University of Bologna. Staff and technicians of LISG are gratefully acknowledged. Kerakoll spa, Sassuolo, Italy, is gratefully acknowledged for providing the composite materials.

7 REFERENCES

Barton, B., Wobbe, E., Dharani, L. R., Silva, P., Birman, V., Nanni, A., Tunis, G. (2005). “Characterization of reinforced concrete beams strengthened by steel reinforced polymer and grout (SRP and SRG) composites.” Materials Science and Engineering: A, 412(1), 129-136.

Balsamo, A., Nardone, F., Iovinella, I., Ceroni, F., & Pecce, M. (2013). Flexural strengthening of concrete beams with EB-FRP, SRP and SRCM: Experimental investigation. Composites Part B: Engineering, 46, 91-101.

Bencardino, F., & Condello, A. (2014). “Structural behaviour of RC beams externally strengthened in flexure with SRG and SRP systems.” International Journal of Structural Engineering, 5(4), 346-368.

Bizindavyi, L., & Neale, K. W. (1999). “Transfer lengths and bond strengths for composites bonded to concrete.” Journal of composites for construction, 3(4), 153-160.

Carloni, C., & Subramaniam, K. V. (2010). Direct determination of cohesive stress transfer during debonding of FRP from concrete. Composite Structures, 93(1), 184-192.

Casadei, P., Nanni, A., & Alkhrdaji, T. (2005). “Steel-reinforced polymer: An innovative and promising material for strengthening infrastructures.” Concrete Engineering International, 9(1), 54-56.

CEN, EN 12390-3, 2009. Testing hardened concrete - Part 3: Compressive strength of test specimens. A1: 2011. Brussels: CEN.

CEN, EN 12390-6, 2009. Testing hardened concrete - Part 6: Tensile splitting strength of test specimens.

Chajes, M. J., Finch, W. W., Januszka, T. F., & Thomson, T. A. (1996). “Bond and force transfer of composite material plates bonded to concrete.” ACI structural journal, 93(2), 208-217.

Dai, J. G., & Ueda, T. (2003, July). “Local bond stress slip relations for FRP sheets-concrete interfaces.” In Proc. of 6th international symposium on FRP reinforcement for concrete structures (pp. 143-152).

Dai, J., Ueda, T., & Sato, Y. (2005). “Development of the nonlinear bond stress–slip model of fiber reinforced plastics sheet–concrete interfaces with a simple method.” Journal of Composites for Construction, 9(1), 52-62.

De Santis, S., de Felice, G., Napoli, A., & Realfonzo, R. (2016). “Strengthening of structures with Steel Reinforced Polymers: A state-of-the-art review.” Composites Part B: Engineering, 104, 87-110.

Elices, M., Guinea, G. V., & Planas, J. (1992). “Measurement of the fracture energy using three-point bend tests: Part 3—influence of cutting the P-δ tail.” Materials and Structures, 25(6), 327-334.

Hillerborg, A. (1985). “The theoretical basis of a method to determine the fracture energy GF of concrete.” Materials and structures, 18(4), 291-296.

Hoover, C. G., & Bažant, Z. P. (2013). “Comprehensive concrete fracture tests: size effects of types 1 & 2, crack length effect and postpeak.” Engineering Fracture Mechanics, 110, 281-289.

Huang, X., Birman, V., Nanni, A., & Tunis, G. (2005). Properties and potential for application of steel reinforced polymer and steel reinforced grout composites. Composites Part B: Engineering, 36(1), 73-82.

Kerakoll S.p.A. – web site: <www.kerakoll.com> [accessed March 2017].

Lopez, A., Galati, N., Alkhrdaji, T., & Nanni, A. (2007). “Strengthening of a reinforced concrete bridge with externally bonded steel reinforced polymer (SRP).” Composites Part B: Engineering, 38(4), 429-436.

Matana, M., Nanni, A., Dharani, L., Silva, P., & Tunis, G. (2005, December). Bond performance of steel reinforced polymer and steel reinforced grout. In Proceedings of international symposium on bond behaviour of FRP in structures (BBFS 2005), Hong Kong (pp. 125-132).

Mitolidis, G. J., Salonikios, T. N., & Kappos, A. J. (2012). “Tests on RC beams strengthened at the span with externally bonded polymers reinforced with carbon or steel fibers.” Journal of Composites for Construction, 16(5), 551-562.

Nakaba, K., Kanakubo, T., Furuta, T., & Yoshizawa, H. (2001). “Bond behavior between fiber-reinforced polymer laminates and concrete.” Structural Journal, 98(3), 359-367.

Pecce, M., Ceroni, F., Prota, A., & Manfredi, G. (2006). Response prediction of RC beams externally bonded with steel-reinforced polymers. Journal of Composites for Construction, 10(3), 195-203.

Prota, A., Tan, K. Y., Nanni, A., Pecce, M., & Manfredi, G. (2006). Performance of shallow reinforced concrete beams with externally bonded steel-reinforced polymer. ACI structural journal, 103(2), 163.

Saber, N., Hassan, T., Abdel-Fayad, A. S., & Gith, H. (2008, July). “Flexural behavior of concrete beams strengthened with steel reinforced polymers.” In Proceedings of the Fourth International Conference on FRP Composites in Civil Engineering, CICE.

Santandrea, M.; Imohamed, I. A. O.; Jahangir, H.; Carloni, C.; Mazzotti, C.; De Miranda, S.; Ubertini, F.; Casadei, P., An investigation of the debonding mechanism in steel FRP- and FRCM-concrete joints, in: 4th Workshop on The New Boundaries of Structural Concrete, Anacapri, September 29th – October 1st, 2016, pp. 289 – 298.

Santandrea, M., Carloni, C., & Wendner, R. “An investigation on the “width and size effect” in the evaluation of the fracture energy of concrete”. Procedia Structural Integrity. 3, 450-458.

Savoia, M., Ferracuti, B., & Mazzotti, C. (2003). “Nonlinear bond-slip law for FRP-concrete interface.” In Proc. of 6th international symposium on FRP reinforcement for concrete structures. Singapore: World Scientific Publications (pp. 163-72).

Täljsten, B. (1997). “Defining anchor lengths of steel and CFRP plates bonded to concrete.” International Journal of Adhesion and Adhesives, 17(4), 319-327.

Taerwe, L., & Matthys, S. (2013) "Fib model code for concrete structures 2010".

Wobbe, E., Silva, P., Barton, B. L., Dharani, L. R., Birman, V., Nanni, A., Tunis, T. (2004, May). “Flexural capacity of RC beams externally bonded with SRP and SRG.” In Proceedings of Society for the Advancement of material and Process Engineering 2004 Symposium (pp. 16-20).